A Study on the β′ and β″ Formation Kinetics in AA6063 Using Differential Scanning Calorimetry

J. van de Langkruis, M.S. Vossenberg, W.H. Kool, and S. van der Zwaag

(Submitted 3 February 2003)

In this work the formation of β″ and β′ precipitates in a commercial AA6063 alloy was investigated using differential scanning calorimetry (DSC) and in situ heat treatments. The DSC used is equipped with fast heating and quenching facilities. The samples were solutionized, isothermally aged to induce formation of β″ or β′, rapidly quenched, and subjected to a DSC scan. The heat treatment cycle was performed entirely in the DSC, to improve the reproducibility of the dissolution and precipitation peaks. The effect of the aging treatment on the size and location of the β″ and β′ peaks was studied. It was found that after aging at 458 K (185 °C) the size of the β″ dissolution peak decreased with aging time, which is correlated with the amount of β″ already precipitated. Similar results were obtained for β′ precipitation at 523 K (250 °C) and 573 K (300 °C). An isothermal transformation diagram for β″ and β′ formation is presented, which is constructed from these experiments. The in situ method proved to be a viable method for studying the transformation sequence and kinetics in this type of alloy.

Keywords Al-Mg-Si, differential scanning calorimetry, isothermal TTT diagram

1. Introduction

The mechanical properties after extrusion of AlMgSi alloys are strongly influenced by the condition of the primary alloying elements Mg and Si in the as-extruded material. Mg and Si should be present in solid solution for optimal strengthening by fine β″-Mg_5Si_6 precipitates during artificial aging,[1] and should not be tied up in relatively large Mg-Si particles formed during cooling of the alloy on exiting the die. Depending on the cooling rate after extrusion, these large particles could be equilibrium β-phase (Mg_2Si) particles or meta-stable β′-phase $Mg_{1.7}Si$ rods.[2] The reduction in matrix solute content due to these large particles causes an undesirable decrease in the amount of strengthening β″ precipitates formed during aging.[2,3]

To predict the amount of precipitates and solute Mg and Si during cooling and aging of the extrusion profile, detailed information about the kinetics of the formation of the specific precipitates is necessary. Many researchers[4-21] have studied the kinetics of the AlMgSi system. One of the main techniques applied to establish the kinetics is differential scanning calorimetry (DSC). With this technique the heat effects involved in the various kinetic reactions are measured in a relatively small sample. With the "classic" approach a new sample is used for each measurement; when the effect of pre-aging on the kinetic reactions is studied, the pre-aging treatments are performed outside the DSC. Due to the sensitivity of the technique and the small heat effects involved, this multi-sample approach gives a considerable scatter in the results.

In this work a new method of applying the DSC technique is presented in which the heat treatments, including homogenization of the sample, are performed in situ. Advantages of the new approach are that effects of compositional differences between samples due to material inhomogeneity are absent, and that the reproducibility and fine detail of the DSC scans improve. Using this approach, more accurate kinetic data of β″ and β′ precipitation and dissolution as a function of the pre-aging treatment are obtained.

J. van de Langkruis (presently at Corus Research, Development and Technology, IJmuiden, The Netherlands); **M.S. Vossenberg** (presently at Corus Aluminium Duffel, Duffel, Belgium); **W.H. Kool,** Laboratory of Materials Science and Technology, Delft University of Technology, Rotterdamseweg 137, 2628 AL, Delft, The Netherlands; and **S. van der Zwaag** (presently at Delft University of Technology, Faculty of Aerospace Engineering, The Netherlands). Contact e-mail: W.H.Kool@tnw.tudelft.nl.

2. Experimental

2.1 Material Preparation

A commercial AA6063 billet with a composition given in Table 1 was homogenized at 843 K (570 °C) for 4 h, quenched with forced air, and subsequently extruded to rectangular profile with cross section 100 mm × 30 mm. From the center of this profile, disc-shaped samples with a diameter of 5 mm and a thickness of about 0.6 mm were machined. The samples weighed 42 ± 1 mg.

2.2 Heat Treatments

The experiments consisted of a solutionizing treatment at 853 K (580 °C) for 1 h and a subsequent quench, in most cases followed by a pre-aging treatment. Nearly all solutionizing

Table 1 Alloy Composition, wt.%

Mg	Si	Fe	Cu, Mn, Cr, Zr, Pb	Ti
0.45	0.40	0.19	<0.01	0.01

Table 2 Heat Treatments Applied After Solutionizing and Phases Expected to Form During Pre-Aging

Experiment	Quench Method	Pre-Aging Time	Phase Formed During Pre-Aging		
			β″	β′	β
No pre-aging	WQ or ZQ		…	…	…
Pre-aging at 458 K	DQ	20 min; 2, 4, 6, 24, 48 h	X	…	…
Pre-aging at 523 K	DQ	15, 30, 45 min; 1, 6, 36 h	X	X	…
Pre-aging at 573 K	DQ	15, 30, 45 min; 1, 6 h	X	X	…
Pre-aging at 640 K	DQ	1, 3, 10, 20 min; 13.3 h	…	X	X

WQ: water quench, ZQ: in situ quench to 273 K, and DQ: in situ quench to the pre-aging temperature

treatments were carried out in situ in the DSC, but some experiments were performed in a vertical tube furnace. The quench after solutionizing was either in situ quenching to 273 K (ZQ) or in situ down quenching to the pre-aging temperature (DQ), or in case of homogenization in the vertical tube furnace, water quenching to 283 K (WQ). The in situ quenching proceeded with ~200 K/min. Pre-aging was performed at various temperatures and times, and after pre-aging the sample was quenched to 273 K with ~200 K/min. The heat treatments are summarized in Table 2. The phases expected to form are also given in this table. For the pre-aging experiments only one sample was used, which was resolutionized in situ before a new pre-aging treatment.

2.3 DSC Experiments

The experiments were performed with a PerkinElmer DSC7 (PerkinElmer, Shelton, CT), using 27 ml/min of 99.998% N_2 gas to avoid further oxidation of the sample. The general shape of the baseline was determined by recording a DSC run with two empty cup holders. An optimal baseline was constructed for each DSC curve, considering a good fit at those temperatures at which no precipitation or dissolution peaks were present.

During the DSC-run the heat flow, dH/dt, is measured as a function of temperature at constant heating rate. After subtracting the selected baseline, the peak area belonging to the heat effect of the transformation, Q_{PEAK}, is calculated with

$$Q_{PEAK} = \int_{T_0}^{T_F} \frac{dH}{dt} \frac{1}{\Phi} dT \quad \text{(Eq 1)}$$

where T_0 and T_F denote the start and finishing temperature of the transformation, and Φ the heating rate dT/dt.

The DSC-run was made with a fixed heating rate of 10 K/min. When two precipitation peaks overlapped, they were separated using the non-linear version of Marquardt's method of a least-squares error fit. The fraction transformed during pre-aging is quantified as follows. The condition of 0% transformed during pre-aging corresponds to that of the maximum exothermic (precipitation) heat effect measured during the DSC-scan after zero quenching, Q_{ZQ}, whereas the condition of 100% transformed corresponds to the endothermic (dissolution) effect after over-aging, Q_{OV}. The fraction transformed during pre-aging, y, is given by

$$y = (Q_{ZQ} - Q_{PEAK})/(Q_{ZQ} - Q_{OV}) \quad \text{(Eq 2)}$$

Q_{ZQ} is negative, Q_{OV} is positive, and Q_{PEAK} may be negative (precipitation) or positive (dissolution). Plotting y against time enables the determination of the time at 10%, 50%, or 90% transformation.

3. Results

Figure 1 shows a typical thermogram after homogenization and in situ zero quenching (ZQ). There are two overlapping exothermic peaks at 558 K and 585 K, one exothermic peak at 693 K, and two endothermic peaks at 658 K and 765 K. Based on the literature[5-11] the three exothermic peaks are attributed to β″-, β′-, and β-precipitation and the two endothermic peaks to β′- and β-dissolution.

3.1 Effects of Pre-Aging on DSC Curve

3.1.1 Pre-Aging at 458 K. Figure 2(a) shows the decrease of the β″ precipitation peak and its change into a β″ dissolution peak with increasing pre-aging time at 458 K. The transition time from precipitation into dissolution is close to 6 h. The dissolution peak does not change with prolonged aging after 24 h, which indicates that after 24 h the structure of the sample has become over-aged. The decrease of the β″ precipitation peak arises from an increase in volume fraction of β″, β′, and/or β precipitates during pre-aging. A dissolution peak appears when sufficient β″ is formed during pre-aging. With increasing pre-aging time, the β″-peak shifts to lower temperatures and the separation between the β″- and the β′ peaks becomes clearer.

Taking into account the overlapping contribution of the β″ peak, it is deduced that the area of the β′ precipitation peak remains approximately constant at pre-aging times up to 6 h and decreases significantly after pre-aging for 24 h. This indicates that no β′ and/or β are formed during pre-aging at shorter times and that β′ and/or β are formed at longer times. However, the β peak is not influenced significantly by the pre-aging time and remains close to that found after zero quenching, which indicates that no appreciable amount of β is formed during pre-aging. Considering the behavior of all three precipitation peaks it is concluded that during pre-aging at 458 K for shorter times (up to ~ 6 h), β″ precipitates are formed, and that for longer times (up to ~ 24 h) further β″ and β′ precipitates are formed.

3.1.2 Pre-Aging at 523 K. Figure 2b shows that after 15 min the β″ peak has already disappeared completely. A possible explanation is that during pre-aging at 523 K so much

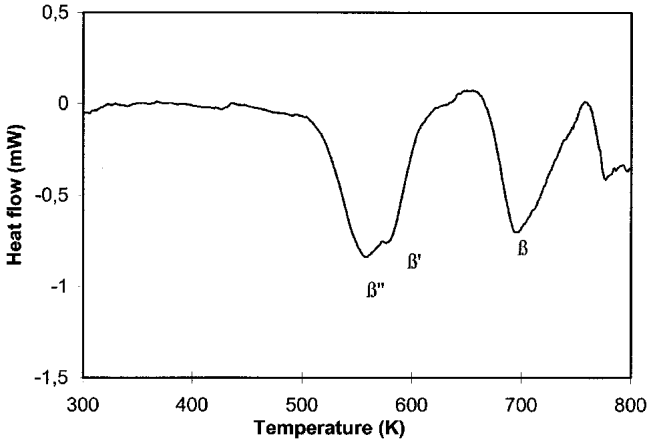

Fig. 1 DSC curve directly after in situ quenching to 273 K (DQ), heating rate 10 K/min

β′′ was formed that the driving force has become too low for further precipitation of β′′ during the DSC scan. An alternative explanation might be that during pre-aging existing β′′ precipitates, formed during down-quenching (see Section 3.1.3), transformed into β′. The presence of a certain amount of β′ precipitates promotes the precipitation of β′, and therefore suppresses the formation of the less stable β′′ during the DSC scan.

The β′ peak area remains constant for pre-aging times up to 15 min and then decreases. The transition time from β′ precipitation into β′ dissolution is slightly less than 1 h. After 36 h pre-aging, the onset temperature of the dissolution peak approaches the pre-aging temperature, indicating that an equilibrium amount of β′ was formed. Although the β′ peak area remains constant up to 15 min pre-aging, the combined heat effect of β′′ and β′ is lower than in the case of ZQ, which means that in that temperature range the total amount of precipitation during the DSC scan is also lower.

There is no significant β′ peak shift with pre-aging time and the shape of the β′ dissolution peaks is not as sharp as that of the β″ dissolution peaks after pre-aging at 458 K. The β peaks are not influenced significantly by the pre-aging time and the peak areas are close to those after zero quenching.

Considering the behavior of the precipitation peaks, two alternative explanations are still possible. First, similar to the conclusions for pre-aging at 458 K, at 523 K for shorter times (smaller than ~ 15 min), β″ precipitates are formed and during prolonged aging (higher than 15 min) only β′ precipitates are formed. Second, for short times no β″ precipitates are formed, but existing β″ precipitates, which were formed during quenching, transform into β′. Consequently, only the β′ phase precipitates.

3.1.3 Pre-Aging at 573 K. After pre-aging at 573 K (Fig. 2c), no β″ peaks were observed. The height of the β′ peak has considerably decreased for the sample pre-aged for 15 min. The transition time from β′ precipitation into β′ dissolution is 15-30 min. As with 523 K, the onset of the β′ dissolution peak approaches the pre-aging temperature. Comparing the β′ dissolution peaks in Fig. 2(b) and (c), it is concluded that their position and shape are strongly determined by the pre-aging temperature. This temperature affects the size of the β′ particles and consequently their dissolution. The β peaks are not influenced significantly by the pre-aging time. Considering the behavior of the precipitation peaks it is concluded that during pre-aging at 573 K only β′ precipitates are formed.

3.1.4 Pre-aging at 640 K. Figure 2(d) indicates that after pre-aging for short times (1-3 min), a β″ precipitation peak is still visible and that the β′ precipitation peak has decreased only slightly. Apparently, during these very short times no significant transformations occurred in the sample. After 10 min, both the β′ and β precipitation peaks have decreased, which indicates β formation during pre-aging at this temperature. After 20 min, the β′ and β precipitation peaks have almost disappeared and no β′ dissolution peak became apparent. This means that after 20 min pre-aging only β precipitates are present. After 13.3 h pre-aging, only a strong β dissolution peak is visible and all β has precipitated. The onset of the peak equals the pre-aging temperature.

3.2 Effect of the Quench Rate

The influence on the DSC curve of the quench rate after homogenization is given in Fig. 3. In this figure the WQ curve, obtained after homogenization and water quenching in a separate furnace, is compared with the ZQ curve, obtained after in situ quenching in the DSC apparatus. The area of the β″ peak of the WQ condition is ~20% bigger than that of the ZQ condition. The other precipitation peak areas are not influenced significantly. Apparently, during quenching in the DSC some β″ precipitation occurred. In the WQ curve an effect of possible GP zone/cluster formation, which is often found in 6xxx alloys with some higher Mg and/or Si content,[10,14,21] is not observed.

4. Discussion

4.1 Peak Assignment and Peak Position

Figure 4 represents the results of a literature survey on temperature ranges for β′′, β′, and β precipitation, obtained from DSC measurements.[5-9,11,12,14] Also, the formation temperatures found in this study and the pre-aging temperatures applied are indicated in this figure. Because the formation temperatures found in this study agree well with those reported, we consider the assignment of the peaks of Fig. 1—although indirect—justified.

Table 3 summarizes the type of the precipitating phases formed at the different pre-aging temperatures. Clear evidence of β′′ formation during pre-aging was only found at 458 K. Although Fig. 4 allows β′′ precipitation at 523 K, we have no preference for one of the alternatives for shorter times, the alternatives being either β′′ precipitation or β′′ transformation into β′.

Formation of β′ during pre-aging was observed at the temperatures 458 K, 523 K, and 573 K (at 458 K for longer times only). Formation of β was only observed at 640 K. The trends in Table 3 agree with those following from Fig. 4, taking into account that the formation of specific phases will also occur at lower temperatures than those derived from DSC experiments, due to the longer times involved with pre-aging.

In most cases peak positions are relatively stable as a func-

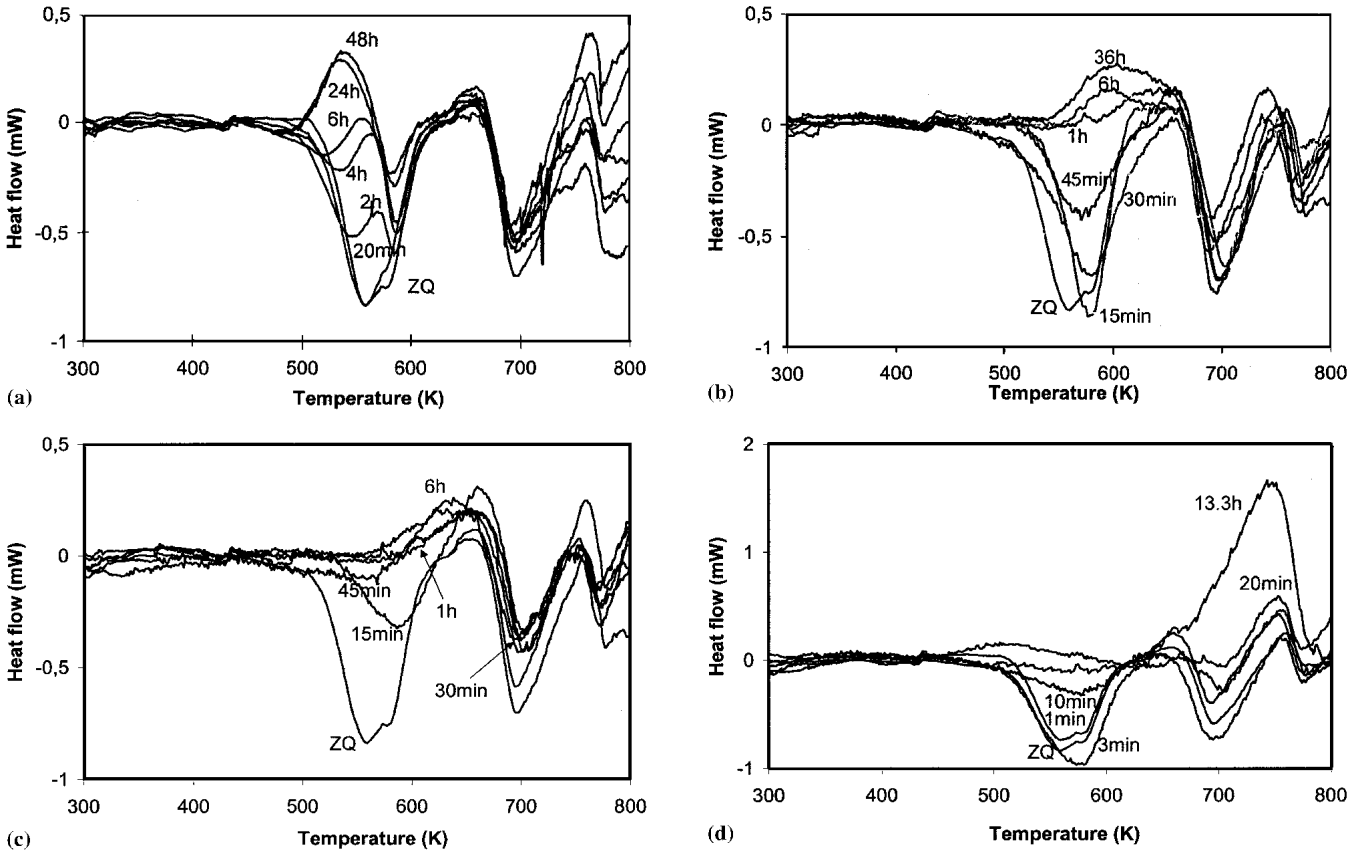

Fig. 2 DSC curves for different pre-aging times at **(a)** 458 K, **(b)** 523 K, **(c)** 573 K, and **(d)** 640 K

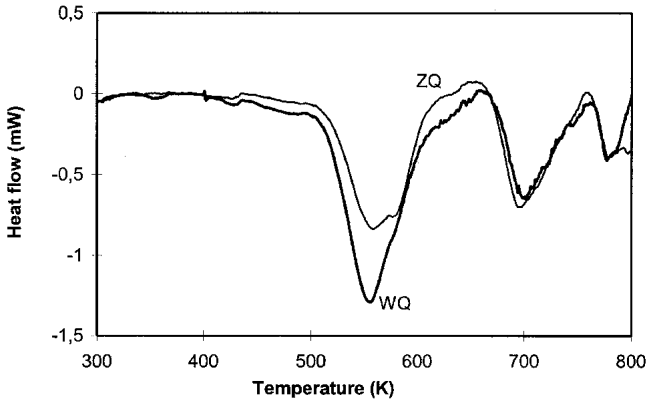

Fig. 3 Influence of the quench rate on the DSC curve; ZQ: zero quenched; WQ: water quenched

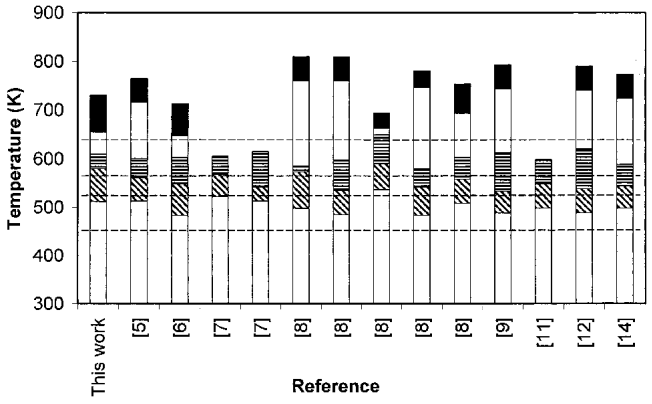

Fig. 4 Temperature regimes reported in the literature for β′′ (▨), β′ (▤), and β (■) precipitation. Temperature regimes found in this study are also indicated. Horizontal lines indicate the pre-aging temperatures used in this study.

tion of pre-aging. There are, however, some exceptions. As a function of pre-aging time at 458 K, the β′′ precipitation peak shifts to lower temperatures, indicating that with the presence of a certain amount of β′′ precipitates, further precipitation of β′′ becomes easier. In contrast, at 458 K and 523 K, the β′ precipitation peak does not shift, indicating that nucleation is easy and that possibly growth onto existing precipitates is dominant. As previously mentioned, the position of the β′ dissolution peaks is strongly determined by the pre-aging temperature, due to different β′ sizes.

4.2 TTT-Diagram

From the curves in Fig. 2, transformation times required to form 10%, 50%, or 90% of the precipitates were derived using Eq 2 and a curve fitting procedure, applying Johnson-Mehl-Avrami-type kinetics. In the method used to calculate the transformation rates the ZQ condition is taken as the 0% transformation reference. During zero quenching some β′′

Table 3 Overview of the Phases Formed at the Different Pre-Aging Temperatures

Precipitate	458 K	523 K	573 K	640 K
β″	Yes	Possible only for short times	No	No
β′	At longer times	Yes	Yes	No
β	No	No	No	Yes

precipitation occurred (Fig. 3). Note that during water quenching a significant amount of vacancies are "frozen in," which will influence the precipitation kinetics, because the driving force for precipitation increases by the presence of excess vacancies and a higher Mg and Si solute content. The ZQ condition, which corresponds with a quenching speed of about 200 K/min applied to a small specimen, is considered a good reference for many circumstances in practice where larger products are quenched.

The transformation times are plotted in Fig. 5 in the form of a TTT-diagram. As too few data points for β formation were obtained, only the curves for β′′ and β′ are given. The times corresponding to 10% β′′ formation are not given, due to the high inaccuracy. There is a general trend of increasing transformation rate with increasing temperature.

In contrast with Fig. 5, TTT-diagrams given in the literature, including those for Al alloys,[22,23] are in most cases constructed from hardness or strength data. In Fig. 6 such a TTT-diagram is given for an AA6xxx-type alloy with a composition close to that of the alloy investigated in this work.[23] The diagram shows that the hardness after artificial aging decreases with pre-aging time. At temperatures below 600 K, this is attributed to the β′ precipitation such as presented in the transformation curves in Fig. 5. Precipitation of β′ during pre-aging reduces the amount of β′′ precipitation during artificial aging and the obtainable strength. The β′ transformation points found in this study are included in the figure except from the 90% transformation point at 523 K. This point (at 10 h) would fall on the (extrapolated) 40 HV contour.

The data points for 10%, 50%, and 90% transformation lie on the iso-hardness contours for 60 HV, 55 HV, and 50-40HV, respectively, which supports the idea of the correspondence between the β′ transformation and the obtainable hardness after artificial aging. Deviations may occur because the alloy compositions and heat treatment procedures were not identical.

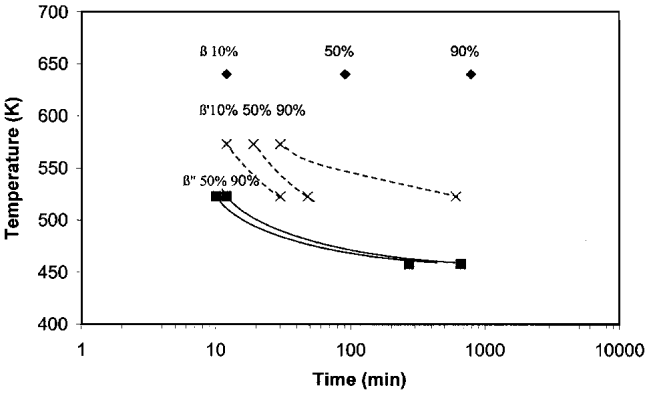

Fig. 5 TTT-diagram for β′′ and β′ precipitation. The data points constitute 50% and 90% transformation of β′′ (■) and 10%, 50%, and 90% transformation of β′ (×). Data for β (◆) precipitation are also included. The lines indicate the expected trends.

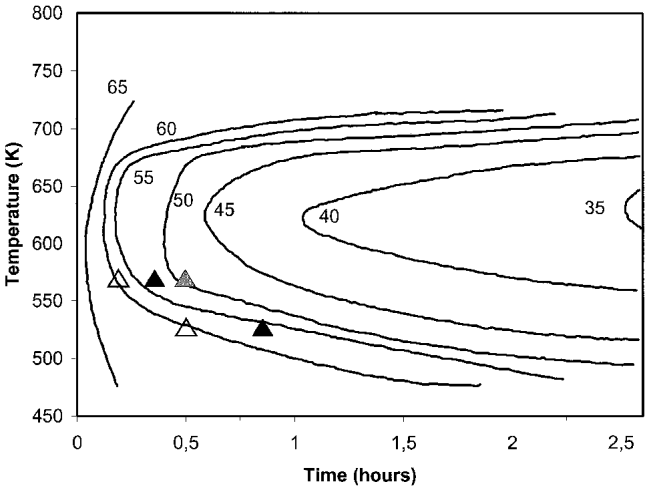

Fig. 6 TTT-diagram for a commercial AlMgSi alloy, composition: 0.44% Mg, 0.36% Si, 0.07% Mn, 0.17% Fe (wt.%) taken from Ref. 23; β′ transformation points in this study: △, 10%; ▲, 20%; ▲, 90% transformation. Numbers at the curves are Vickers hardness values.

5. Conclusion

Based on the presented work the following conclusions are drawn:

- In situ solutionizing and aging experiments in a DSC with fast heating and quenching capabilities are very suitable to study the precipitation kinetics in AA6xxx alloys. Also, dissolution kinetics can be studied in this way. TTT-diagrams for β″ and β′ formation could be constructed based on the changes in peak area.
- The TTT-diagram constructed in this way is comparable to a TTT-diagram of a similar alloy, reported in the literature and constructed from hardness measurements.
- As a function of pre-aging the β′′ precipitation peak shifts, in contrast to the β′ precipitation peak. This finding implies that the influence of nucleation is dominant in β′′ precipitation and negligible in β′ precipitation.

Acknowledgments

The authors acknowledge the financial support of the Technology Foundation. The authors thank Mr. N. Geerlofs for technical support and Mr. Chen Shangping for valuable discussions. The authors thank Boal Profielen B.V. for supplying the extruded material.

References

1. S.J. Andersen, H.W. Zandbergen, J. Jansen, C. Traeholt, U. Tundal, and O. Reiso: *Acta Mater.*, 1998, *46*(9), pp. 3283-90.

2. S. Zajac, B. Bengtsson, A. Johansson, and L.-O. Gullman: *Mater. Sci. Forum,* 1996, *217-222,* pp. 397-402.
3. D. Marchive and P. Faivre: *Light Met. Age,* 1983, *41*, pp. 6-10.
4. K. Matsuda, S. Ikeno, T. Sato, and A. Kamio: *Proc. Recent Metallurgical Advances in Light Metal Industries*, Canadian Institute of Mining, Metallurgy and Petroleum, Montreal, Canada, 1995, pp. 465-72.
5. M. Takeda, F. Okhubo, T. Shirai, and K. Fukui: *J. Mater. Sci.,* 1998, *33,* pp. 2385-90.
6. S.B. Kang, L. Zhen, H.W. Kim, and S.T. Lee: *Mater. Sci. Forum,* 1996, *217-222,* pp. 827-32.
7. M. Saga, Y. Sasaki, M. Kikuchi, Z. Yan, and M. Matsuo: *Mater. Sci. Forum,* 1996, *217-222,* pp. 821-26.
8. K. Gupta and D.J. Lloyd: *Proc. 3rd Int. Conf. on Aluminium Alloys, Their Physical and Mechanical Properties*, L. Arnberg, O. Lohne, E. Nes, and N. Ryum, ed., Trondheim, Norway, 1992, pp. 21-26.
9. J. Polmear: *Proc. 3rd Int. Conf. on Aluminium Alloys, Their Physical and Mechanical Properties,* L. Arnberg, O. Lohne, E. Nes, and N. Ryum, ed., Trondheim, Norway, 1992, pp. 371-85.
10. S.P. Chen, K.M. Mussert, and S. van der Zwaag: *J. Mater. Sci.,* 1998, *33,* pp. 4477-83.
11. J.D. Bryant: in *Proc. Conf. on Automotive Alloys*, S.K. Das and G.J. Kipouros, ed., The Minerals, Metals and Materials Society, Warrendale, PA, 1997, pp. 19-35.
12. I. Dutta and S.M. Allen: *J. Mater. Sci. Lett.,* 1991, *10*(6), pp. 323-27.
13. D.G. Eskin, V. Massardier, and P. Merle: *J. Mater. Sci.,* 1999, *34,* pp. 811-20.
14. G.A. Edwards, K. Stiller, G.L. Dunlop, and M.J. Couper: *Mater. Sci. Forum,* 1996, *217-222,* pp. 713-18.
15. F.J. Vermolen: "Mathematical Models for Particle Dissolution in Extrudable Aluminum Alloys," Ph.D. Thesis, Delft University of Technology, Delft University Press, Delft, The Netherlands, 1998.
16. H. Westengen and N. Ryum: *Z. Metallkde,* 1979, *70*(8), pp. 528-35.
17. I. Kovács, J. Lendvai, and E. Nagy: *Acta Metall.,* 1972, *20,* pp. 975-83.
18. J.P. Lynch, L.M. Brown, and M.H. Jacobs: *Acta Metall.,* 1982, *30,* pp. 1389-95.
19. M.H. Jacobs: *Philos. Mag.,* 1972, *26*(1), pp. 1-13.
20. K. Matsuda, S. Ikeno, T. Sato, and A. Kamio: *Mater. Sci. Forum,* 1996, *217-222,* pp. 707-12.
21. A.K. Gupta, D.J. Lloyd, and S.A. Court: *Mater. Sci. Eng.,* 2001, *A301,* pp. 140-46.
22. G.F. Vander Voort, ed.: *Atlas of Time-Temperature Diagrams for Non-Ferrous Alloys,* ASM International, Materials Park, OH, 1991.
23. J. Bryant, D.J. Field, and E.P. Butler: Alcan Int., European Patent no. 0 222 479 B1, 1989.